IEEE Access
Multidisciplinary | Rapid Review | Open Access Journal

Received August 30, 2021, accepted September 12, 2021, date of publication September 20, 2021,
date of current version September 28, 2021.

Digital Object Identifier 10.1109/ACCESS.2021.3114220

A Numerical Research on a New Type of Asteroid Flexible Probe

WEIFENG YAN AND HEXI BAOYIN
School of Aerospace Engineering, Tsinghua University, Beijing 100084, China
Corresponding author: Hexi Baoyin (baoyin@tsinghua.edu.cn)

This work was supported by the National Key Research and Development Program of China under Grant 2019YFA0706500.

ABSTRACT The asteroid landing detection is of great scientific and economic value. The traditional landing rigid probe is prone to rebound and escape due to the asteroid's weak gravity and rugged terrain. Flexible body can avoid these problems by its deformation energy dissipation and ability to recovery. To promote the development of asteroid detection, this paper proposes a new type of flexible asteroid landing probe and demonstrates its advantages and feasibility. Firstly, this paper establishes a theory of asteroid's dynamics environment with the polyhedron method and the spherical harmonic method. Secondly, this paper uses the discrete shell model to calculate the flexible probe's internal force, the spring damping model and viscous-sliding friction model for its external force. Thirdly, this paper builds the flexible landing dynamics equations and achieves the dynamics simulation of the flexible probe. Finally, this paper demonstrates the advantages and feasibility of the flexible probe through two landing examples.

INDEX TERMS Asteroid exploration, dynamics, flexible probe, landing detection.

I. INTRODUCTION

Asteroid detection is one of the most valuable and difficult researches in aerospace science. It is very likely that asteroids originated from planetary collisions and bursts in ancient times [1]. By detecting the structure and internal matter of asteroids, humans can obtain information about the evolution of the solar system and even the origin and development of the universe. In addition to research value, asteroids also have great economic value for its rich rare metal [2]. What's more, asteroids could be used as the propellants supply depot for future deep space exploration missions. Current asteroid detection methods include surround detection, short-range leap detection, landing detection. However, only landing detection is feasible to realize the above-mentioned values of asteroids.

In recent years, with the development of aerospace technology, many countries have carried out asteroid detection. Since the 20th century, there have been more than 20 asteroid-related missions, but only three missions have achieved asteroid landing, which are Japanese Hayabusa probe, European Rosetta probe and American OSIRIS Rex probe. Launched in May 2003, reaching the target asteroid Ishikawa in September 2005, the Japanese Hayabusa 1 probe achieved the first-ever sampling of asteroid surface material and successfully sent the sample to the earth in June 2010 [3], [4]. However, the Minerva landing probe released by Hayabusa 1 failed to land on the asteroid due to the weak gravity of Ishikawa. Following Hayabusa 1, the Hayabusa 2 asteroid probe was launched in December 2014, reaching the target asteroid 1999JU3 in 2018 [5]. It successfully took samples of the interior of asteroids in addition to surface material and sent the samples to the earth. Besides that, its Minerva probe also achieved a successful landing, which the Hayabusa 1 probe failed to do. However, both Hayabusa 1 and Hayabusa 2 did not achieve a steady landing and they sampled by a brief collision with target asteroids [6], [7]. The European Rosetta probe was launched in March 2004 and approached the target comet Chury in August 2014 and successfully achieved a stable orbit around the target comet [8]. In November 2014, the Rosetta probe released the Philae landing probe which tried to land on the surface of the comet through a special harpoon tripod fixation anchoring system [9]. Unfortunately, the Philae anchoring system did not achieve the expected effect on the complex surface of the asteroid, causing it to fall in the absence of sunlight and lose contact. NASA's OSIRIS Rex probe was launched in September 2016 and approached

The associate editor coordinating the review of this manuscript and approving it for publication was Halil Ersin Soken.

the target asteroid Bennu in December 2018 [10], [11]. In July 2020, the OSIRIS Rex detector touched the surface of Bennu through a robotic arm and successfully collected samples [12], [13]. However, OSIRIS Rex landed for such a short time that it was not a landing detection so much as a contact detection.

From the three asteroid landing exploration missions above, it can be seen that stable landing on the surface of the asteroid is still faced with lots of difficulties, which mainly lies in the weak gravity and rugged terrain of the asteroid. Due to the limited size of the asteroid probe and in order not to contaminate the samples, the probe usually lands on the asteroid's surface through hard landing [14]. However, by hard-landing, the probe is prone to rebound and escape in a weak gravity [4]. At the same time, the rugged terrain of the asteroid and lack of corresponding information make it difficult to determine the landing point so that the probe is prone to overturning [15]. In general, the asteroid landing detection is still challenging and worth further research.

In the past research, some scholars have proposed some new asteroid landing detection plans. Yongbin *et al.* [16] and Zhao *et al.* [17] proposed an improved asteroid anchoring system based on the Philae anchoring system respectively. NASA also proposed an anchoring attachment system based on elastic elements. However, all of these anchoring systems adopt mechanical fixation with rigid structure, and face the same problem encountered by the Philae probe.

Compared with the rigid structure, the flexible structure can effectively avoid the rebound and escape caused by hard landing in weak gravity with the flexible energy dissipation mechanism. The deformation recovery ability also makes it better adaptable to rugged terrain of asteroids. With above advantages, the probe with flexible material as main structure is expected to become a new generation of asteroid landing probe. In order to promote the development of asteroid detection, this paper proposes a new type of flexible probe (shown in the fig.4), which consists of a flexible base with a 1m diameter and three rigid masses for protecting payloads.

To verify the advantages and feasibility of the flexible probe, it is essential to establish a dynamics model of the process when the flexible probe lands on the asteroid. In this regard, there are many relevant studies. For instance, Yoshikawa [7] *et al.* recommended a detailed study on the Hayabusa 2's trajectory and attitude on the asteroid, which conduced to the subsequent asteroid landing. Zhang *et al.* [18] also proposed a model of asteroid dynamics environment and demonstrated the feasibility of a flexible net spacecraft. In addition, Si *et al.* [19] studied the attachment and collision theory of the flexible bodies, and put forward a flexible net for space capture. What's more, Zhang *et al.* [20] used the nonlinear spring damping method and Hertz contact theory to study the collision of flexible bodies and made a research on the control rate of space flexible capture. Gingold *et al.* [21] proposed an efficient modeling method for large-deformation flexible bodies, which provided a theoretical basis for numerical study of the flexible probe.

The flexible probe in this paper includes flexible part and rigid part. Different from the Earth environment, the working environment is the rugged asteroid surface with a weak gravity. Considering that, there are still many problems to be solved in the dynamics study of the flexible probe. First of all, how to model the complex interaction between the flexible probe and the asteroid [18] ? Secondly, how's the cushioning effect of the flexible probe under a weak gravity?

To solve problems above, this paper proposes a new type of flexible asteroid landing probe and a corresponding dynamics theory, demonstrating the advantages and feasibility of such probe through numerical simulation. The second section establishes the theory of asteroid's dynamics environment, including the asteroid gravity and rugged terrain. The third section introduces the flexible asteroid probe, building the flexible landing dynamics equations. The fourth section demonstrates the advantages and feasibility of flexible probe through numerical simulation. The fifth part introduces the conclusion of this paper.

II. DYNAMICS ENVIRONMENT OF THE ASTEROID

The asteroid dynamics environment is the foundation of the dynamics of the flexible probe. When the probe approaches the asteroid, it will be affected by the gravity of the asteroid, planets nearby and the sun, as well as the light pressure. Studies have shown that only the influence of the asteroid gravity need to be considered for short-term orbiting and landing detection within the Hill radius of the asteroid. Therefore, this paper mainly considers the asteroid gravity and surface model.

A. THE ASTEROID GRAVITY MODEL

Originating from computer graphics, the polyhedron method has been widely used for gravity model of irregular asteroids. This method uses triangles as the basic unit to simulate the complex surface of the asteroid. Through integral transformation, the gravitational potential energy of the asteroid is expressed as functions related to the units and their edges. This study takes asteroid Bennu as the target. Fig.1(a) shows the polyhedral model of Bennu [22]. This polyhedral model disintegrates Bennu into 2692 triangular units and 4038 edges.

According to the polyhedron method, the formula of the gravitational potential per unit mass and gravity is as follows:

$$\begin{aligned} U(\boldsymbol{r}) &= \frac{1}{2}\mathrm{G}\rho \sum_{e\in ES} \boldsymbol{r}_{er}^{T}\left(\boldsymbol{n}_{f_1}\left(\boldsymbol{n}_e^{f_1}\right)^{T} + \boldsymbol{n}_{f_2}\left(\boldsymbol{n}_e^{f_2}\right)^{T}\right)\boldsymbol{r}_e L_e \\ &\quad - \frac{1}{2}G\rho \sum_{f\in FS} \boldsymbol{r}_{fr}^{T}\left(\boldsymbol{n}_f\left(\boldsymbol{n}_f\right)^{T}\right)\boldsymbol{r}_{fr}\boldsymbol{\omega}_f \\ \nabla U(\boldsymbol{r}) &= \mathrm{G}\rho \sum_{e\in ES}\left(\boldsymbol{n}_{f_1}\left(\boldsymbol{n}_e^{f_1}\right)^{T} + \boldsymbol{n}_{f_2}\left(\boldsymbol{n}_e^{f_2}\right)^{T}\right)\boldsymbol{r}_e L_e \\ &\quad - G\rho \sum_{f\in FS} \boldsymbol{n}_f\left(\boldsymbol{n}_f\right)^{T}\boldsymbol{r}_{fr}\boldsymbol{\omega}_f \end{aligned} \tag{1}$$

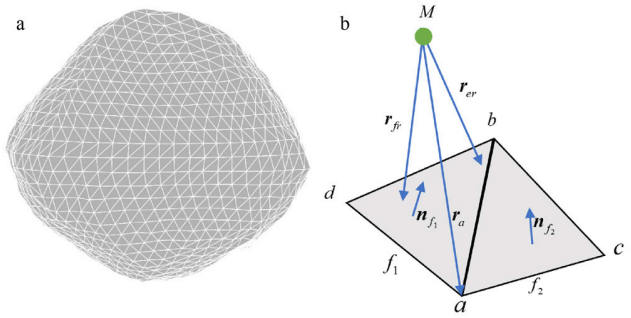

FIGURE 1. The polyhedral model of Bennu. (a) The whole units of Bennu. (b) Any two units of Bennu.

where G is the gravitational constant, ρ is the asteroid's density, FS is the set of all polyhedral units, ES is the set of all edges of the units, $\boldsymbol{r}_{er}$ is the vector from the target point M to any point of the edge e, $\boldsymbol{r}_{fr}$ is the vector from the target point M to any point of the unit f. f_1 and f_1 are the units which have the public edge e. $\boldsymbol{n}_{f_1}$ and $\boldsymbol{n}_{f_2}$ is the unit normal vector of the unit f_1 and f_2 respectively, and both of them point to the outside of the asteroid. $\boldsymbol{n}_e^{f_1}$ is the unit normal vector which lies in the unit f_1 and is perpendicular to the edge e and points to d. $\boldsymbol{n}_e^{f_2}$ is the unit normal vector which lies in the unit f_2 and is perpendicular to the edge e and points to c. L_e and ω_f are the dimensionless coefficients of the unit, and the formula is:

$$L_e = \ln\left(\frac{r_a + r_b + e_{ab}}{r_a + r_b - e_{ab}}\right)$$
$$\omega_f = 2\arctan\left(\frac{\boldsymbol{r}_a \cdot (\boldsymbol{r}_b \times \boldsymbol{r}_c)}{r_a r_b r_c + r_a(\boldsymbol{r}_b \cdot \boldsymbol{r}_c) + r_b(\boldsymbol{r}_c \cdot \boldsymbol{r}_a) + r_c(\boldsymbol{r}_a \cdot \boldsymbol{r}_b)}\right) \tag{2}$$

where $\boldsymbol{r}_a, \boldsymbol{r}_b, \boldsymbol{r}_c$ are the vectors from the target point M to point a, b, c respectively, e_{ab} is the distance between point a and c. For the symbols above, please refer to Fig.1(b).

Fig.2 shows the distribution of gravitational potential per unit mass and gravity magnitude on the asteroid Bennu.

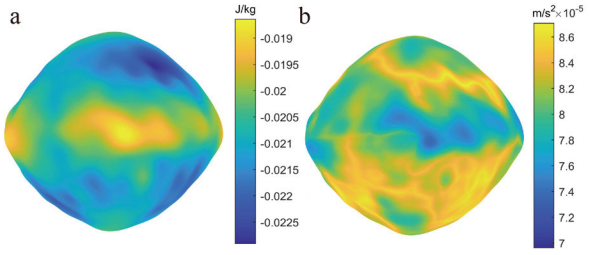

FIGURE 2. (a) Gravitational potential per unit mass of Bennu. (b) Gravity magnitude of Bennu.

B. THE ASTEROID SURFACE MODEL

The surface model is the first step for the study of collisions between the flexible probe and asteroids. In this paper, the spherical harmonic method is used to reconstruct the irregular surface of asteroids. This method converts the surface into the spherical harmonics, and get a continuous parameter model through the survey points on the asteroid surface. With the continuous model, the information required for collision modeling can be easily obtained.

In order to ensure that the surface parameter model will not change with the movement of the asteroid, this paper adopts the satellite coordinate system, which take the asteroid's centroid as the coordinate origin, the principal axis of minimum inertia as the x axis, and the principal axis of maximum inertia as the z axis. The y axis and the x, z axis form a right-handed system. In this coordinate system, the formula is as follows:

$$R(\theta, \varphi) = \sum_{n=0}^{\infty} \sum_{m=-n}^{n} C_n^m Y_n^m(\theta, \varphi) \quad \theta \in [0, \pi], \ \varphi \in [0, 2\pi] \tag{3}$$

where $R(\theta, \varphi)$ is the radial distance from the origin to the surface, θ, φ are the zenith angle and the azimuth angle of the spherical coordinates on the asteroid, and C_n^m is the spherical harmonic complex coefficients, $Y_n^m(\theta, \varphi)$ is the spherical harmonic basis function, which can be determined according to the accuracy of the solution. The formula for any order is as follows:

$$Y_n^m(\theta, \varphi) = \sqrt{\frac{2n+1}{4\pi} \cdot \frac{(n-m)!}{(n+m)!}} P_n^m(\cos\theta) e^{im\varphi} \tag{4}$$

where $P_n^m(\cdot)$ is the Legendre polynomials, i is the imaginary unit, e is the base of natural logarithms. Legendre polynomials of any order are as follows:

$$P_n^m(\cos\theta) = \frac{(-1)^m}{2^n n!} \left(1 - \cos^2\theta\right)^{m/2} \frac{d^{n+m}}{dx^{n+m}} \left(\cos^2\theta - 1\right)^n \tag{5}$$

According to (3)(4)(5), the distance at any position of the asteroid surface to the centroid can be obtained. The normal and tangential information of the asteroid surface can be calculated by (3). Suppose $\hat{\boldsymbol{r}}$ is the unit vector from the centroid to the asteroid surface, then the position vector at this place is $\boldsymbol{R} = R\hat{\boldsymbol{r}}$, so the tangent vectors $\boldsymbol{\tau}_1$, $\boldsymbol{\tau}_2$ at this place and the normal vector $\boldsymbol{\lambda}$ can be calculated as follows:

$$\begin{cases} \boldsymbol{\tau}_1 = \dfrac{\partial R}{\partial \theta}\hat{\boldsymbol{r}} + R\dfrac{\partial \hat{\boldsymbol{r}}}{\partial \theta} \\ \boldsymbol{\tau}_2 = \dfrac{\partial R}{\partial \varphi}\hat{\boldsymbol{r}} + R\dfrac{\partial \hat{\boldsymbol{r}}}{\partial \varphi} \\ \boldsymbol{\lambda} = \boldsymbol{\tau}_1 \times \boldsymbol{\tau}_2 \end{cases} \tag{6}$$

Combining (3)(4)(5)(6), the normal information and tangential information of the asteroid surface can be obtained. Fig.3 shows the surface of the Bennu solved by the spherical harmonic method.

III. THE FLEXIBLE LANDING DYNAMICS

A. THE FLEXIBLE PROBE

The asteroid landing probes before were rigid probes, such as the Minerva and Philae probes mentioned above. In order

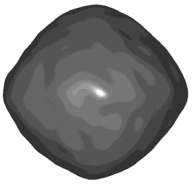

FIGURE 3. The surface of Bennu.

to solve the problem that the rigid probe is prone to rebound and escape due to weak gravity and rugged terrain, this paper proposes a new type of flexible asteroid landing probe. The flexible probe (Fig.4) includes a flexible chassis with a 2m diameter and three rigid masses distributed in the circumferential direction. The flexible chassis is 2cm thick, and the material can be flexible materials such as silicone rubber and vulcanized rubber. The flexible chassis deforms during the landing, which enables the probe to achieve rapid and stable attachment through deformation dissipation and collision dissipation. Due to its large bottom, the flexible detector is not prone to overturning at a large-angle, avoiding being out of control. Embedded in the flexible chassis through the bottom, the mass block contains rigid components such as jets and payloads (See fig.5 for details). The rigid mass block will sample and carry out other detection work after landing and provide control force and control moment when moving on the asteroid.

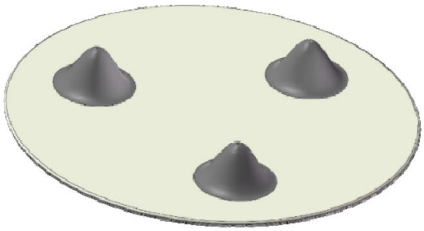

FIGURE 4. The flexible probe.

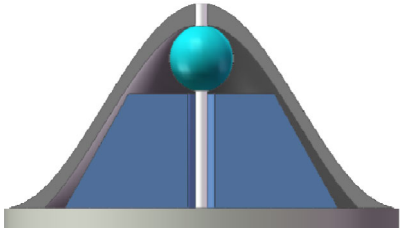

FIGURE 5. The mass block.

In this study, the rigid mass block is 0.6m away from the center of the chassis, and its outer wall is a sinusoidal surface while the shape and position can be adjusted in practice. The following study uses numerical simulation to illustrate the advantages of the flexible probe in detection.

B. DYNAMICS MODEL OF THE FLEXIBLE PROBE

The flexible probe contains both flexible and rigid parts. The flexible part of the probe has the characteristic of shell. Therefore, the traditional finite element method will have numerical divergence when dealing with such problems. In order to establish the dynamics model of the flexible probe, this paper introduces the discrete shell model in differential geometry to model the rigid-flexible coupling of the flexible probe [21], [23]. In this method, the flexible probe is divided into triangular units along the middle plane. The mass of the probe is equivalent to the vertex (mass point) of the triangular unit, and the movement of the probe is equal to the mass point. When the flexible probe deforms, the discrete shell model calculates the internal force by deformation energy, which is divided into membrane energy and bending energy. Fig.6 shows units of the flexible probe. For observation, the flexible part is marked as blue and the rigid part as yellow. The following describes the discrete shell model method.

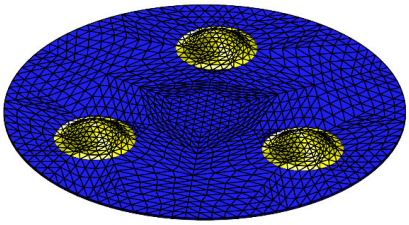

FIGURE 6. The whole units of the flexible probe.

1) MEMBRANE ENERGY

The membrane energy of the flexible body after deformation can be calculated by membrane strain. From the definition of strain, the calculation formula of membrane strain can be as follows:

$$\begin{aligned}\boldsymbol{\varepsilon}_m = \frac{1}{8A^2}\Big[&\left(\tilde{l}_1^2 - l_1^2\right)(\boldsymbol{t}_2 \otimes \boldsymbol{t}_3 + \boldsymbol{t}_3 \otimes \boldsymbol{t}_2) + \left(\tilde{l}_2^2 - l_2^2\right)\cdot \\ &\times (\boldsymbol{t}_1 \otimes \boldsymbol{t}_3 + \boldsymbol{t}_3 \otimes \boldsymbol{t}_1) + \left(\tilde{l}_3^2 - l_3^2\right) \\ &\times (\boldsymbol{t}_1 \otimes \boldsymbol{t}_2 + \boldsymbol{t}_2 \otimes \boldsymbol{t}_1)\Big] \end{aligned} \tag{7}$$

where $\boldsymbol{\varepsilon}_m$ is the membrane strain, A is the area of the triangular unit, l_1, l_2, l_3 represent the length of the triangular unit's each edge respectively, $\tilde{l}_1, \tilde{l}_3, \tilde{l}_3$ represent length of the triangular unit's each edge without deformation respectively. $\boldsymbol{t}_1, \boldsymbol{t}_2, \boldsymbol{t}_3$ are the norm vectors of the unit's edges respectively, lying in the plane of the triangle unit and pointing to the outside of the unit. Their norms are as follows: $\|\boldsymbol{t}_1\| = l_1$, $\|\boldsymbol{t}_2\| = l_2$, $\|\boldsymbol{t}_3\| = l_3$. $(\cdot \otimes \cdot)$ is the dyadic of vectors. The symbols above are shown in the fig.7.

After obtaining the membrane strain, the following formula can be used to calculate the membrane energy:

$$W_m = \frac{\tilde{A}Eh}{2\left(1-\mu^2\right)}\left[(1-\mu)\,Tr\left(\boldsymbol{\varepsilon}_m^2\right) + \mu\left(Tr\left(\boldsymbol{\varepsilon}_m\right)\right)^2\right] \tag{8}$$

where W_m is the membrane energy, $\tilde{A}$ is the area of the triangular unit before deformation, E is the Young's modulus

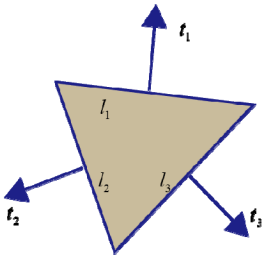

FIGURE 7. One unit for membrane energy.

of the flexible material, μ is the Poisson's ratio of the flexible material, h is the thickness of the flexible body, $Tr(\cdot)$ is the trace of the matrix. Combining (7) and (8), the membrane energy of the flexible body is obtained. It is worth noting that only $\boldsymbol{\varepsilon}_m$ changes in each time step, which means high efficiency of simulation.

2) BENDING ENERGY

The bending energy of the flexible body during the large deformation can be derived from the bending stress which is calculated by the curvature of the middle surface. Though being continuous in space, the curvature of the surface in the triangular units can be converted to the edge, which is convenient for implementation of the program. In the discrete shell model, the curvature is equivalent to the adjacent triangular units' dihedral angle, by which the bending strain is obtained. The formula is as follows:

$$\boldsymbol{\varepsilon}_b = \frac{\left[\Phi\left(\tilde{\theta}\right) - \Phi(\theta)\right]}{2\tilde{A}l}\boldsymbol{s} \otimes \boldsymbol{s} \tag{9}$$

where $\boldsymbol{\varepsilon}_b$ represents the bending strain, θ is the dihedral of the two units, $\tilde{\theta}$ is the dihedral of the two units without deformation, $\tilde{A}$ is the sum of the area when the two triangle units are not deformed, $\boldsymbol{s}$ is the unit vector perpendicular to the adjacent units' average normal and the edge $\boldsymbol{l}$, l is the norm of $\boldsymbol{l}$, and $\Phi(\cdot)$ is the undetermined curvature conversion function. The symbols above are referred to the fig.8.

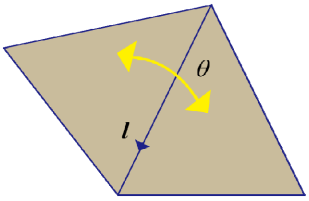

FIGURE 8. The adjacent units for bending energy.

In order to ensure that the equilibrium state is undeformed, it is necessary that $\Phi(\cdot)$ is 0 when the dihedral's change is 0, and $\Phi(\cdot)$ should be an increasing function relative to the dihedral change. Three simple curvature conversion functions are as follows:

$$\Phi(\theta) = \pi - \theta$$
$$\Phi(\theta) = 2\sin\left(\frac{\pi - \theta}{2}\right)$$
$$\Phi(\theta) = 2\tan\left(\frac{\pi - \theta}{2}\right) \tag{10}$$

Considering that the lager the degree is, the more difficult the bending will be, this paper adopts $\Phi(\theta) = 2\tan(\pi/2 - \theta/2)$ as the curvature conversion function. After the function is determined, the Koiter shell model theory is used to calculate the bending energy, and the formula is as follows:

$$W_b = \frac{\tilde{A}Eh^3}{24\left(1-\mu^2\right)}\left[(1-\mu)\,Tr\left(\boldsymbol{\varepsilon}_b^2\right) + \mu\left(Tr\left(\boldsymbol{\varepsilon}_b\right)\right)^2\right] \tag{11}$$

where W_b is the bending energy, E is the Young's modulus of material, μ is the Poisson's ratio, h is the thickness of the flexible body, $Tr(\cdot)$ is the trace of the matrix. In the simulation, only $\boldsymbol{\varepsilon}_b$ needs to be calculated in each time step, and the rest is only related to the undeformed state, which improves the efficiency of simulation calculation.

3) THE INTERNAL FORCE

Equation (8) and (11) can be used to calculate the membrane energy and bending energy of any unit after deformation. The energy of the entire flexible body is as follows:

$$W_{total} = \sum_{i=1}^{Nt} W_{mi} + \sum_{i=1}^{Ne} W_{bi} \tag{12}$$

where W_{total} is the total energy, Nt is the number of triangular units, Ne is the number of units with a common edge, W_{mi} is the membrane energy of the ith unit, W_{bi} is the bending energy of the ith units with a common edge.

With the deformed energy of the flexible body, the internal force can be calculated by the principle of virtual displacement, $\boldsymbol{F}_i^{in} = \partial W_{total}/\partial \boldsymbol{r}_i$. Where $\boldsymbol{F}_i^{in}$ is the internal force of the ith mass point, and $\boldsymbol{r}_i$ is the position vector of the ith mass point.

Since this study adopts the discrete shell model for the rigid and flexible part, it is necessary to verify the accuracy of the model in simulating the two materials. There are two examples to illustrate the accuracy of the discrete shell model. Fig.9 shows the comparison between the fixed-supported rigid beam' deflection curves calculated by the discrete shell model (DSM) and the standard deflection formula respectively. Fig.10 shows the comparison between the simply supported flexible beam's deflection curves calculated by the discrete shell model (DSM) and Abaqus software respectively. Through these two comparisons, it can be seen that the discrete shell model is very accurate in simulation of rigid materials and flexible materials.

C. COLLISION MODEL

When the flexible probe approaches the asteroid, the collision between the asteroid and the probe must be considered. Therefore, a reasonable collision model is of great significance to the selection of the trajectory and

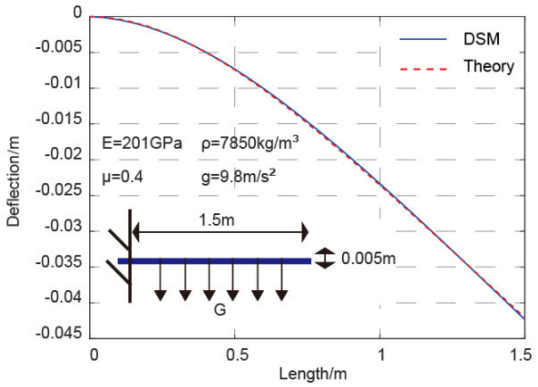

FIGURE 9. The fixed-supported rigid beam.

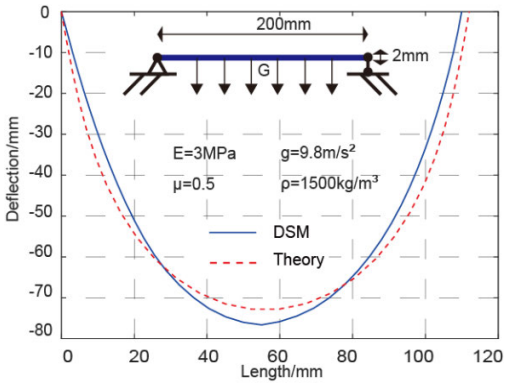

FIGURE 10. The simply supported flexible beam.

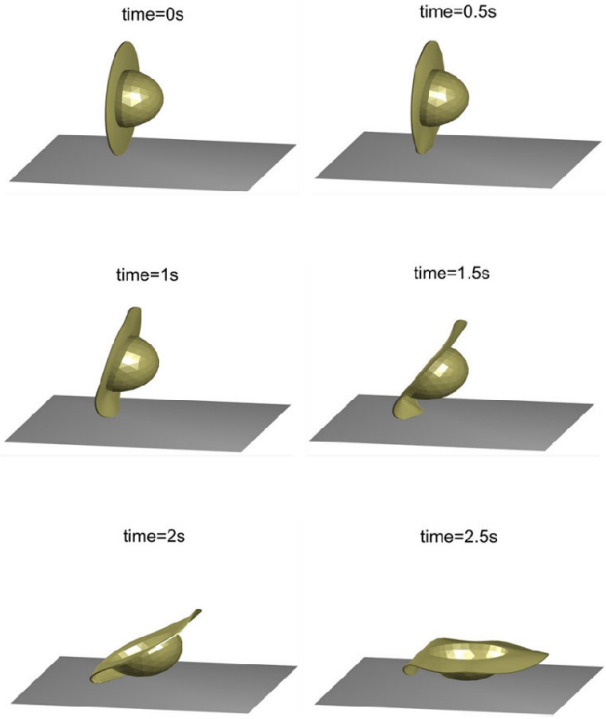

FIGURE 11. The motion of a flexible hat.

landing sites. In this study, the collision between the flexible probe and the asteroid is separated into the collision of the mass point, which can be decomposed into normal collision and tangential collision. Next, this paper introduces the normal collision model and tangential collision model of the flexible body.

1) NORMAL COLLISION

The normal collision force adopts the spring damping model which is based on the Hertz collision and the Hunt-crossly damping theory. Taking the impact of material properties and contact area into consideration, the spring damping model can accurately model the changes of physical quantities such as the speed and displacement of the mass point during the collision process. For each mass point, the formula of the normal collision force is as follows:

$$N = \left(K_n d + C_n \dot{d}\right) \cdot \delta \tag{13}$$

where N is the normal collision force. $d = R(\theta, \varphi) - \|\boldsymbol{r}\|$, where θ, φ are the zenith angle and the azimuth angle of the mass point, and $R(\theta, \varphi)$ is the radial distance from the origin to the asteroid surface, which can be calculated by the method in section II.B. $\dot{d}$ is the normal component of the mass point's velocity on the asteroid surface, and the normal information is detailed in section II.B. δ is the collision function, if $d < 0, \delta = 1$, else $\delta = 1$. K_n is the elastic coefficient, which can be calculated according to the Hertz collision theory, C_n is the damping coefficient, which is determined by K_n and the coefficient of restitution. The formula for K_n and C_n is as follows:

$$\begin{aligned} K_n &= \frac{4}{3}\kappa^* E^* \\ C_n &= -2\sqrt{\frac{K_n m}{\pi^2 + (\ln e)^2}} \ln e \end{aligned} \tag{14}$$

where $\kappa^* = (1/\kappa_1 + 1/\kappa_2)^{-0.5}$, where κ_1 is the curvature radius of the asteroid surface at the collision point, κ_2 is the curvature radius of the mass point, which can be replaced by a smaller fixed value. $E^* = \left(\left(1 - \upsilon_1^2\right)/E_1 + \left(1 - \upsilon_2^2\right)/E_2\right)^{-1}$, where E_1 is the Young's modulus of the asteroid, υ_1 is the Poisson's ratio of the asteroid, E_2 is the Young's modulus of the mass point, and υ_2 is the Poisson's ratio of the mass point. is the mass of the mass point, e is the coefficient of restitution between the mass point and the asteroid, which can be determined through experiments.

2) TANGENTIAL COLLISION

On the asteroid surface, the collision force includes not only the normal collision force, but also the tangential collision force. In this paper, viscous-sliding friction model is used for the tangential collision force of the mass point. The formula

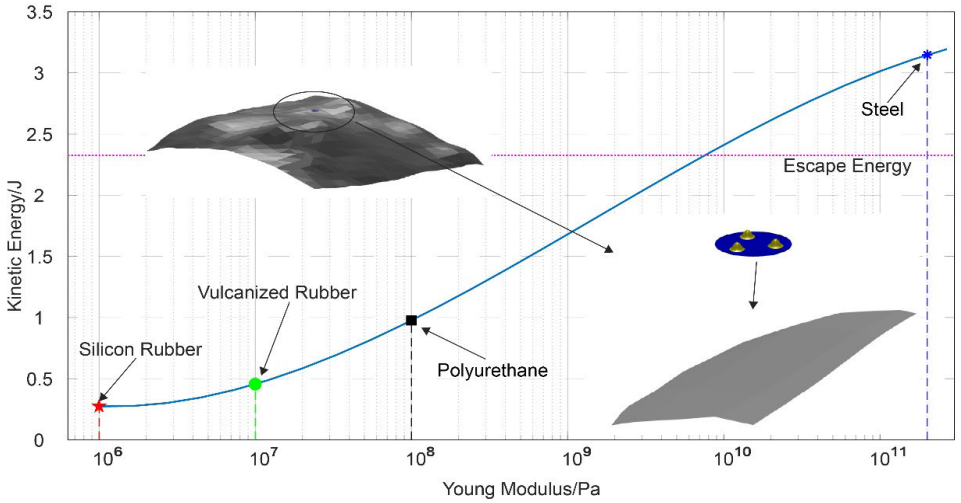

FIGURE 12. The total kinetic energy of the flexible probe after the first collision.

is as follows:

$$f = \begin{cases} \left(K_t \boldsymbol{s} + C_t \dot{\boldsymbol{r}}^{\tau}\right)\delta, & K_t \|\boldsymbol{s}\| < \mu N \\ \left(\mu N \cdot \dfrac{\dot{\boldsymbol{r}}^{\tau}}{\|\dot{\boldsymbol{r}}^{\tau}\|}\right)\delta, & K_t \|\boldsymbol{s}\| \geq \mu N \end{cases} \tag{15}$$

where $\boldsymbol{f}$ is the tangential collision force, $\dot{\boldsymbol{r}}^{\tau}$ is the tangential velocity of the mass point relative to the asteroid surface, the tangential information is detailed in section II.B. δ is the collision function, $\boldsymbol{s} = \int_{t_0}^{t} \dot{\boldsymbol{r}}^{\tau} dt$, where t is the current time and t_0 is the time of the initial collision. K_t is the tangential friction coefficient, C_t is the damping coefficient of tangential friction, and μ is the friction coefficient.

D. THE FLEXIBLE LANDING DYNAMICS EQUATIONS

Combining the internal and the external force with the discrete shell model, the flexible landing dynamic equations in the asteroid's satellite coordinate system is as follows:

$$\begin{cases} m_i \ddot{\boldsymbol{r}}_i = \boldsymbol{F}_i^{ex} + \boldsymbol{F}_i^{in}, \ i = 1, 2, \ldots, Np \\ \boldsymbol{F}_i^{ex} = -m_i \left[2\boldsymbol{\omega} \times \boldsymbol{r}_i + \boldsymbol{\omega} \times (\boldsymbol{\omega} \times \boldsymbol{r}_i)\right] \\ -m_i \nabla U\left(\boldsymbol{r}_i\right) + \left(N_i \cdot \boldsymbol{n}_i - \boldsymbol{f}_i\right) \end{cases} \tag{16}$$

where Np is the number of mass points, m_i is the mass of the ith mass point, ω is the angular velocity of the asteroid's satellite coordinate system relative to the inertial system, $\nabla U\left(\boldsymbol{r}_i\right)$ is the asteroid gravity, $\boldsymbol{f}_i$ is the normal collision force between the mass point and the asteroid, N_i is the tangential collision force, see section III.C. $\boldsymbol{F}_i^{in}$ is the internal force, see section III.B. Due to the difference between the masses, this paper disregards the collision's impact on asteroids as well as the relative and angular acceleration of the asteroid and the probe.

The equations (16) consists of Np second-order differential equations. Combining the initial position and velocity information with RK45 method, the information on the motion of the flexible probe on the asteroid can be obtained. Here equations (16) are applied to the deformation process of a flexible dome straw hat (see fig.11), showing the dynamics accuracy and versatility of the flexible landing dynamic equations.

IV. SIMULATION AND RESULT

The research above has completed the study of the asteroid dynamics' environment and the flexible probe dynamics model, obtaining the flexible landing dynamics equations, which lays a theoretical foundation for the application of the flexible probe in the asteroid landing detection. This chapter completes the simulation of the flexible probe landing on the asteroid, and verifies the advantages and feasibility of the flexible probe.

A. ADVANTAGES OF THE FLEXIBLE PROBE

In order to verify the advantages of the flexible probe in asteroid landing detection, this paper takes Bennu as the target, completing the landing simulation of probes with different flexible materials at a certain initial speed, and comparing the results after the first collision.

The material of the rigid block is steel, whose Young's modulus is 201GPa, Poisson's ratio is 0.28, and the total weight of the three rigid block is 74kg. The Young's modulus of the flexible material is 0.001GPa−300GPa, Poisson's ratio is 0.4, and the total mass of the flexible chassis is 44kg. At the initial moment, the chassis is parallel to the asteroid's equatorial plane and its center is located at [0; 0; 260] m,whose speed is at [0.1; 0.1; −0.5] m/s (equivalent to Philae's landing speed).

In this case, the relationship between the rebound kinetic energy after collision and the Young's modulus of the flexible material is shown in the fig.12. From the figure, it can be seen that the rebound kinetic energy of the probe after a hard landing experiences a significant decrease as the Young's

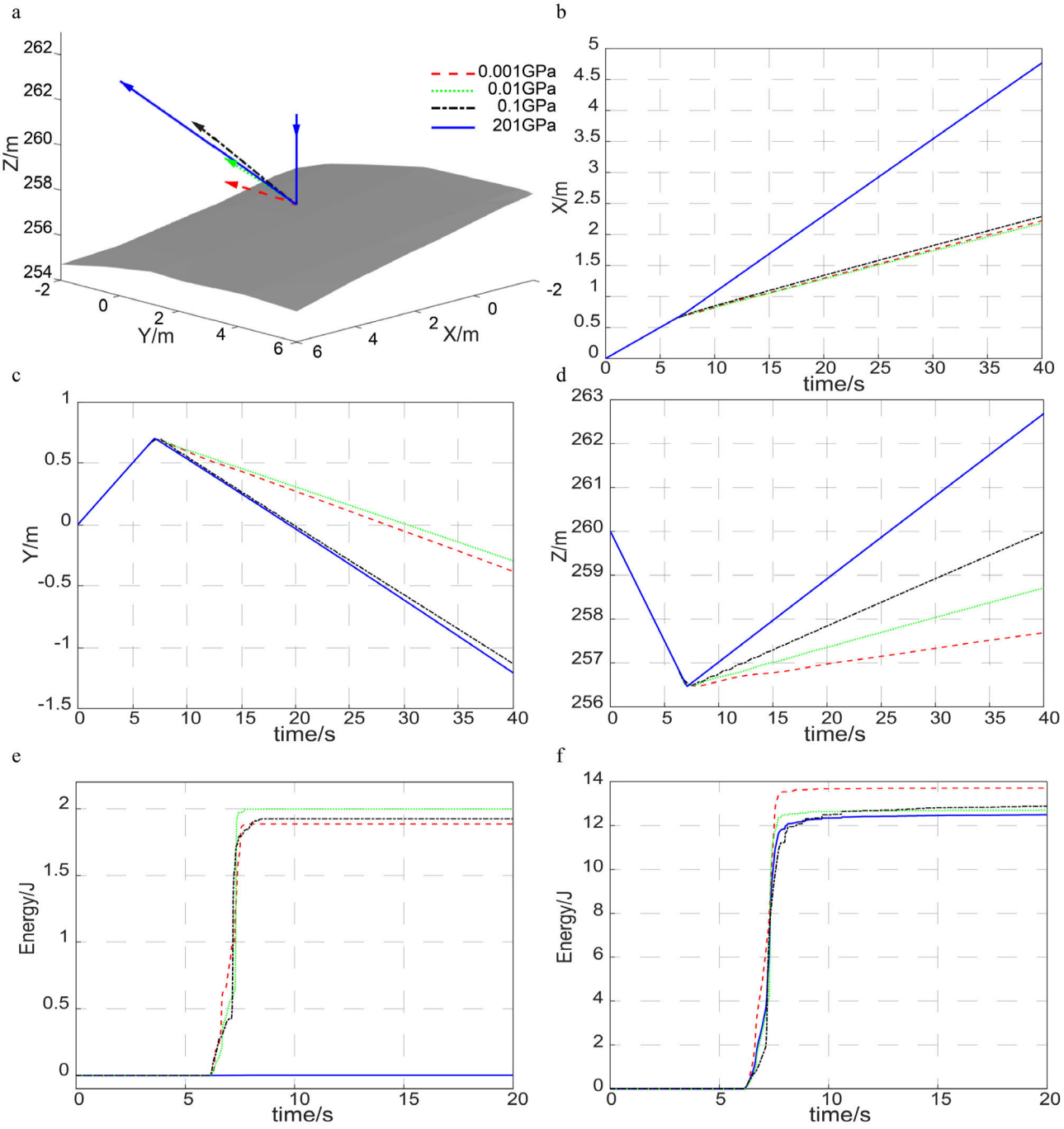

FIGURE 13. Four examples with different materials. (a) Displacement of the flexible probe. (b) Displacement in X-direction. (c) Displacement in Y-direction. (d) Displacement in Z-direction. (e) The material dissipation. (f) The collision dissipation.

modulus decreases. When materials with a small Young's modulus used in the chassis, such as silicon rubber, vulcanized rubber, and polyurethane, the rebound kinetic energy is apparently less than the escape energy, which means that the probe will be captured by the asteroid gravity instead of rebounding and escaping. In contrast, when the chassis is made of rigid materials, such as steel, similar to the current rigid asteroid probe, the rebound kinetic energy is greater than the escape energy so the probe will not be captured by the asteroid gravity, which means a failed mission.

Next the probes with materials of $E = 0.001$GPa, $E = 0.01$GPa, $E = 0.1$GPa, and $E = 201$GPa, which correspond to the three types of flexible materials commonly used in the aerospace field (silicon rubber, vulcanized rubber, polyurethane) and steel, are used to analyze the advantages of the flexible probe. Fig.13(a) shows the displacement of

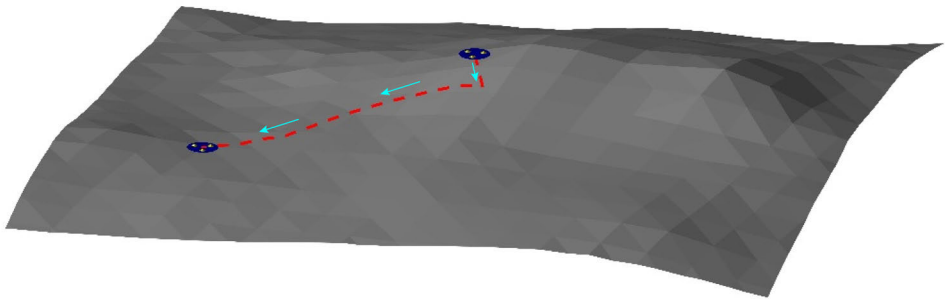

FIGURE 14. The trajectory of the flexible probe.

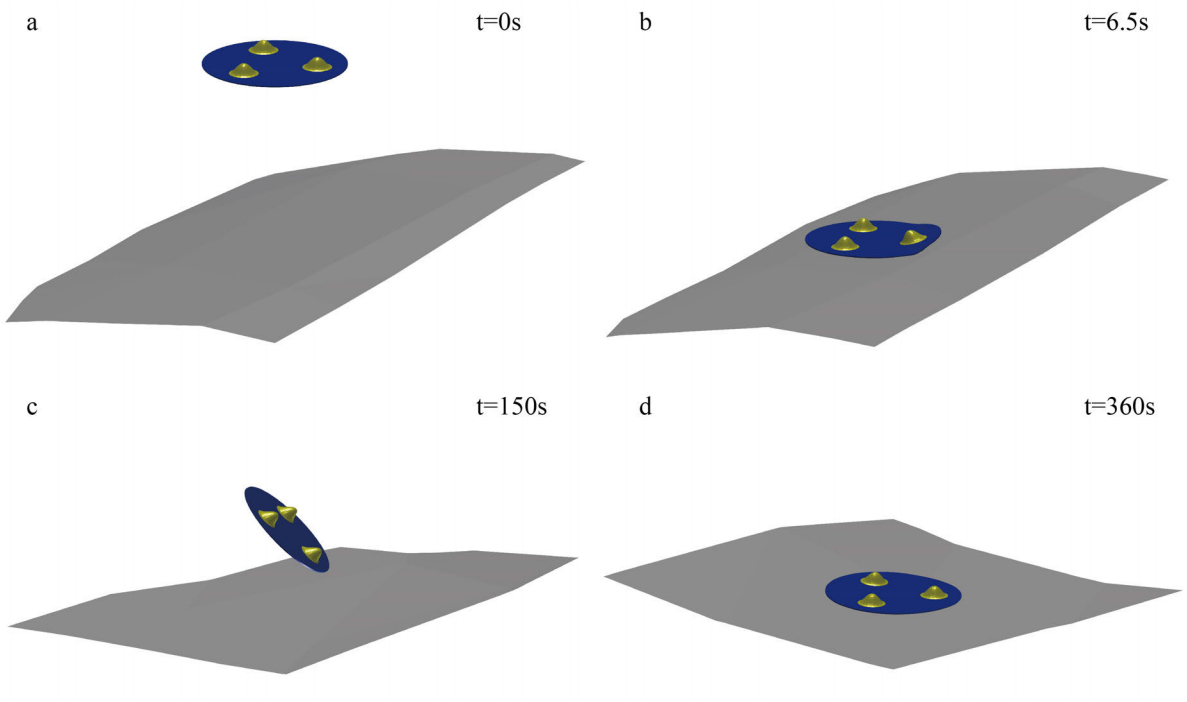

FIGURE 15. (a) The flexible at 0s. (b) The flexible probe at 6.5s. (c) The flexible probe at 150s. (d) The flexible probe at 360s.

the center of the flexible probe with different chassis materials. Fig.13(b) to Fig.13(d) show the changes of the displacement in the X, Y, and Z directions respectively. It can be seen that although the initial state is exactly the same, the probe with flexible material can effectively reduce the tangential velocity during the collision, so as to avoid large tangential displacement. Besides, the smaller the Young's modulus of the material, the better the effect of reducing the tangential velocity is, which ensures that the probe will not deviate too far from the target. In contrast, the probe with material of $E = 201$GPa can hardly reduce the tangential velocity, which means a large drift will occur even if the probe has small tangential velocity. For example, Philae drifted for 1.2km after its anchoring system failed. The flexible probe can also reduce the normal speed, which means higher possibility of a safe asteroid landing. For example, the probes with material of $E = 0.001$GPa, $E = 0.01$GPa, $E = 0.1$GPa do not escape while the rigid probe does. With a rigid probe, additional fixtures or higher delivery accuracy are required, which will bring about more burden to asteroid detection.

Fig.13(e) and fig.14(f) show the comparison of the material dissipation and collision dissipation among four probes, which is another proof of the flexible probe's advantages. During the collision, the flexible probe will deform, increasing the contact area and the collision dissipation. This effect will be more distinctive as the material becomes more flexible. More importantly, the deformation of flexible material will also bring additional material dissipation, which is close to 0 in rigid probe.

In general, through hard landing on the asteroid, the flexible probe has greater energy dissipation, less prone to rebound and escape, closer to the target point, compared with the traditional probe.

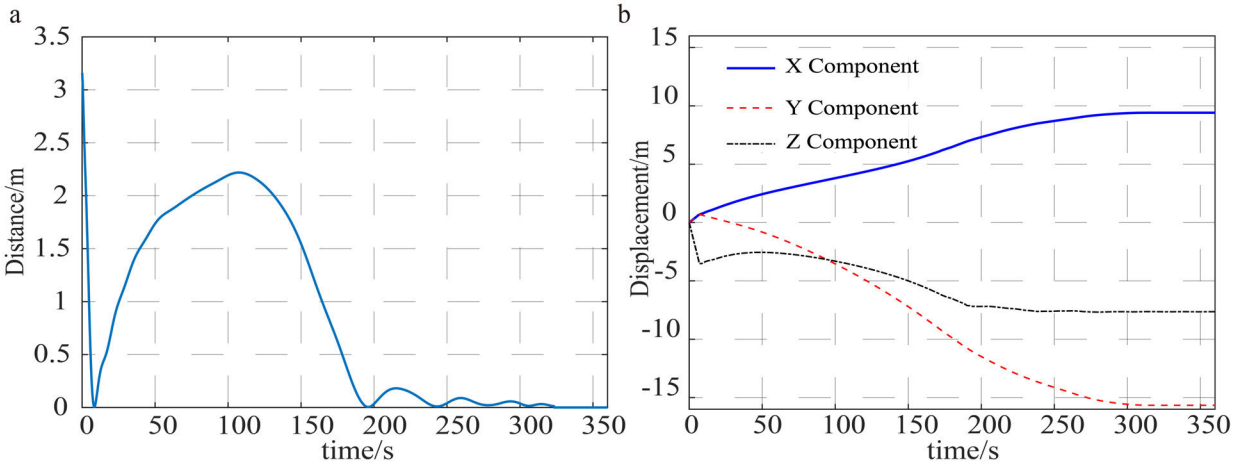

FIGURE 16. (a) Distance between the flexible probe and Bennu. (b) Displacement of the flexible probe.

B. SUCCESSFUL LANDING OF THE FLEXIBLE PROBE

In order to verify the feasibility of the flexible probe, this paper completes a simulation in which the flexible probe successfully lands on the asteroid. The material of the rigid block is steel, whose Young's modulus is 201GPa, Poisson's ratio is 0.28, and the total weight of the three rigid block is 74kg. The chassis material is silicon rubber, whose Young's modulus is 0.001GPa, Poisson's ratio is 0.4, and the total mass of the flexible chassis is 44kg. At the initial moment, the chassis is parallel to the asteroid's equatorial plane and its center is located at [0; 0; 260] m, whose speed is at [0.1; 0.1; −0.5] m/s. The simulation duration is 360s.

Fig.14 shows the trajectory of the flexible probe on the asteroid. Fig.15 show the state of the flexible probe at 0s, 6.5s, 150s, and 360s. Fig.16(a) shows the variation of the chassis center's displacement component. Fig.16(b) shows the change in the distance between the chassis center and the surface of the asteroid.

Figures show that under the conditions above, the flexible probe collides with the asteroid for the first time at 6s and then leaves the asteroid. At 185s, 235s, 270s and 310s, the flexible probe collides with the asteroid again and lands stably at 325s. From the first collision to the stable landing, the flexible probe bounces for 6 minutes. It is 19.0366m between the initial collision point and the final landing point. In addition, the flexible probe doesn't overturn finally.

In general, the flexible probe can achieve asteroid hard landing.

V. CONCLUSION

This paper proposes a new type of flexible asteroid landing probe and the corresponding dynamic theory, providing a new plan for asteroid landing detection. Studies in this paper shows that, compared with the rigid probe, the flexible probe can reduce its energy faster through material and collision dissipation when landing on the asteroid, avoiding rebound and escape. Therefore, the flexible probe can land on asteroids through a simple hard landing without additional control or fixed devices, which is of great potential. In the following research, it is necessary to study the impact of the flexible probe's structure on landing, including the distribution of the rigid mass block, the shape and thickness of the flexible chassis and so on. In addition, it is necessary to study the criterion which ensures a safe landing. Last but not least, how the flexible probe uses jet devices to perform large-scale movement on the asteroid needs further study.

ACKNOWLEDGMENT

Special thanks to J. Xiao and Y. Zhang for their suggestions on language polishing.

REFERENCES

[1] J. C. Castillo-Rogez, M. Pavone, I. A. D. Nesnas, and J. A. Hoffman, "Expected science return of spatially-extended *in-situ* exploration at small Solar system bodies," in *Proc. IEEE Aerosp. Conf.*, Mar. 2012, pp. 1–5, doi: 10.1109/AERO.2012.6187034.

[2] A. Peloni, M. Ceriotti, and B. Dachwald, "Solar-sail trajectory design for a multiple near-earth-asteroid rendezvous mission," *J. Guid., Control, Dyn.*, vol. 39, no. 12, pp. 2712–2724, Dec. 2016, doi: 10.2514/1.G000470.

[3] A. Fujiwara, J. Kawaguchi, D. K. Yeomans, M. Abe, T. Mukai, T. Okada, J. Saito, H. Yano, M. Yoshikawa, D. J. Scheeres, and O. Barnouin-Jha, "The rubble-pile asteroid Itokawa as observed by Hayabusa," *Science*, vol. 312, no. 5778, pp. 1330–1334, Jun. 2006, doi: 10.1126/science.1125841.

[4] M. Yoshikawa, J. Kawaguchi, and H. Kuninaka, "The results of asteroid exploration mission Hayabusa," *IEICE Tech. Rep.*, vol. 110, no. 7, pp. 219–222, 2010, doi: 10.1002/gps.4244.

[5] M. Yoshikawa, J. Kawaguchi, A. Fujiwara, and A. Tsuchiyama, "The Hayabusa mission," in *Sample Return Missions*. Amsterdam, The Netherlands: Elsevier, 2021, ch. 6, pp. 123–146, doi: 10.1016/B978-0-12-818330-4.00006-9.

[6] T. Kubota, M. Otsuki, and T. Hashimoto, "Touchdown dynamics for sample collection in Hayabusa mission," in *Proc. IEEE Int. Conf. Robot. Automat.*, May 2008, pp. 158–163, doi: 10.1109/ROBOT.2008.4543202.

[7] K. Yoshikawa, H. Sawada, S. Kikuchi, N. Ogawa, Y. Mimasu, G. Ono, Y. Takei, F. Terui, T. Saiki, S. Yasuda, K. Matsushima, T. Masuda, and Y. Tsuda, "Modeling and analysis of Hayabusa2 touchdown," *Astrodynamics*, vol. 4, no. 2, pp. 119–135, Jun. 2020, doi: 10.1007/s42064-020-0073-x.

[8] V. A. Dorofeeva, "Chemical and isotope composition of comet 67P/Churyumov—Gerasimenko: The Rosetta—Philae mission results reviewed in the context of cosmogony and cosmochemistry," *Sol. Syst. Res.*, vol. 54, no. 2, pp. 96–120, Mar. 2020, doi: 10.1134/S0038094620020021.

[9] E. Hand, "Philae probe makes bumpy touchdown on a comet," *Science*, vol. 346, no. 6212, pp. 900–901, Nov. 2014, doi: 10.1126/science.346.6212.900.
[10] J. A. Ansari and R. Umar, "NASA's OSIRIS-REx spacecraft enters close orbit around Bennu, breaking record," *Hydroresearch*, 2019.
[11] B. Zhang and Y. Cai, "Immersion and invariance based adaptive backstepping control for body-fixed hovering over an asteroid," *IEEE Access*, vol. 7, pp. 34850–34861, 2019, doi: 10.1109/ACCESS.2019.2904590.
[12] D. S. Lauretta, S. S. Balram-Knutson, E. Beshore, W. V. Boynton, C. D. d'Aubigny, D. N. DellaGiustina, H. L. Enos, D. R. Golish, C. W. Hergenrother, E. S. Howell, and C. A. Bennett, "OSIRIS-REx: Sample return from asteroid (101955) Bennu," *Space Sci. Rev.*, vol. 212, nos. 1–2, pp. 925–984, Oct. 2017, doi: 10.1007/s11214-017-0405-1.
[13] S. R. Chesley, D. Farnocchia, M. C. Nolan, D. Vokrouhlický, P. W. Chodas, A. Milani, F. Spoto, B. Rozitis, L. A. M. Benner, W. F. Bottke, M. W. Busch, J. P. Emery, E. S. Howell, D. S. Lauretta, J.-L. Margot, and P. A. Taylor, "Orbit and bulk density of the OSIRIS-REx target asteroid (101955) Bennu," *Icarus*, vol. 235, pp. 5–22, Jun. 2014, doi: 10.1016/j.icarus.2014.02.020.
[14] Z. Zhao, S. Yin, Q. Sun, Z. Yin, D. Liu, H. Yu, N. Zhang, J. Li, Z. Yao, C. Chao, and T. Zhang, "Gas-driven regolith-sampling strategy for exploring micro-gravity asteroids," *IEEE Access*, vol. 8, pp. 56191–56202, 2020, doi: 10.1109/ACCESS.2020.2982290.
[15] F. Wu and Y. Fan, "Optical imaging instruments and main science results of small body exploration: A review," *IEEE Access*, vol. 9, pp. 78973–78992, 2021, doi: 10.1109/ACCESS.2021.3084456.
[16] W. Yongbin, J. Wansong, L. Long, Z. Qian, F. Rui, and W. Liwu, "Design and experimental research of a new type of asteroid anchoring system," *Int. J. Aerosp. Eng.*, vol. 2021, pp. 1–7, May 2021, doi: 10.1155/2021/6677877.
[17] Z. Zhao, J. Zhao, and H. Liu, "Development of a landing mechanism for asteroids with soft surface," *Int. J. Aerosp. Eng.*, vol. 2013, pp. 1–9, 2013, doi: 10.1155/2013/873135.
[18] Y. Zhang, Y. Yu, and H. Baoyin, "Dynamical behavior of flexible net spacecraft for landing on asteroid," *Astrodynamics*, vol. 2021, pp. 1–3, Mar. 2021, doi: 10.1007/s42064-021-0102-4.
[19] J. Si, Z. Pang, Z. Du, and J. Fu, "Dynamics modeling and simulation of a net closing mechanism for tether-net capture," *Int. J. Aerosp. Eng.*, vol. 2021, pp. 1–16, Jan. 2021, doi: 10.1155/2021/8827141.
[20] F. Zhang, P. Huang, Z. Meng, Y. Zhang, and Z. Liu, "Dynamics analysis and controller design for maneuverable tethered space net robot," *J. Guidance Control Dyn.*, vol. 40, no. 11, pp. 1–16, 2017, doi: 10.2514/1.G002656.
[21] Y. Gingold, A. Secord, J. Y. Han, E. Grinspun, and D. Zorin, "A discrete model for inelastic deformation of thin shells," in *Proc. ACM SIGGRAPH/Eurograph. Symp. Comput. Animation*, 2004, pp. 1–12.
[22] M. C. Nolan, C. Magri, E. S. Howell, L. Benner, and D. J. Scheeres, "Asteroid (101955) bennu shape model V1.0," Nasa Planet. Data Syst., Tech. Rep. EAE-A-I0037-5-BENNUSHAPE-V1.0, Sep. 2013.
[23] E. Grinspun, "A discrete model of thin shells," *Birkhäuser Basel*, vol. 38, pp. 325–337, 2008, doi: 10.1007/978-3-7643-8621-4_17.

WEIFENG YAN received the B.S. degree in engineering from Tsinghua University, China, in 2021, where he is currently pursuing the master's degree. His current research interests include asteroid landing detection and flexible probes.

HEXI BAOYIN is currently a Professor at Tsinghua University. His current research interests include orbit theory in irregular gravitational fields, and interplanetary mission analysis and optimization.